ARTICLE

Electrobiofabrication of antibody sensor interfaces within a 3D printed device yield rapid and robust electrochemical measurements of titer and glycan structure

Chen-Yu Chen[1,2,3] | Dana Motabar[1,2,3] | Fauziah Rahma Zakaria[1,2,3] | Eunkyoung Kim[2,3] | Benjamin Wu[1,2,3] | Gregory F. Payne[2,3] | William E. Bentley[1,2,3]

[1]Fischell Department of Bioengineering, University of Maryland, College Park, Maryland, USA

[2]Institute for Bioscience and Biotechnology Research, University of Maryland, College Park, Maryland, USA

[3]Robert E. Fischell Institute for Biomedical Devices, University of Maryland, College Park, Maryland, USA

Correspondence
William E. Bentley, Fischell Department of Bioengineering, University of Maryland, College Park, MD, 20742, USA.
Email: bentley@umd.edu

Abstract

We report the integration of 3D printing, electrobiofabrication, and protein engineering to create a device that enables near real-time analysis of monoclonal antibody (mAb) titer and quality. 3D printing was used to create the macroscale architecture that can control fluidic contact of a sample with multiple electrodes for replicate measurements. An analysis "chip" was configured as a "snap-in" module for connecting to a 3D printed housing containing fluidic and electronic communication systems. Electrobiofabrication was used to functionalize each electrode by the assembly of a hydrogel interface containing biomolecular recognition and capture proteins. Specifically, an electrochemical thiol oxidation is used to assemble a thiolated polyethylene glycol hydrogel, that in turn is covalently coupled to either a cysteine-tagged protein G that binds the antibody's Fc region or a lectin that binds the glycans of target mAb analytes. We first show the design, assembly, and testing of the hardware device. Then, we show the transition of a step-by-step sensing methodology (e.g., mix, incubate, wash, mix, incubate, wash, measure) into the current method where functionalization, antibody capture, and assessment are performed in situ and in parallel channels. Both titer and glycan analyses were found to be linear with antibody concentration (to 0.2 mg/L). We further found the interfaces could be reused with remarkably similar results. Because the interface assembly and use are simple, rapid, and robust, we suggest this assessment methodology will be widely applicable, including for other biomolecular process development and manufacturing environments.

KEYWORDS
3D printed sensors, antibody sensing, electrobiofabrication, electrochemical sensing

1 | INTRODUCTION

The development process for antibody therapeutics is both costly and time-consuming owing to the complexities of optimizing host cell lines, bioreactors, processing conditions, and product characterization (Rodrigues et al., 2010; Shukla et al., 2017; Steinmeyer & McCormick, 2008). Measurement tools that rapidly and accurately assess the production process and product quality are of great interest as they can speed development times. Further, if sufficiently robust, they could open doors towards optimal control of manufacturing processes (Gerzon et al., 2022). The concentration of antibody per liter of cell culture broth (i.e., titer) is one such critical process parameter (CPP); it is needed to characterize upstream production efficiency (Langer & Rader, 2015). Product quality, formally a critical quality attribute, is assessed in many ways, one being an antibody's glycan structure. To the best of our knowledge, there are no measurement tools that provide both titer and glycan assessment in simple, easy-to-use formats that directly provide electronic output in real time. Moreover, while biological recognition elements offer tremendous selectivity and sensitivity, their incorporation into sensing systems is extremely challenging and this limits their widespread use.

Microfluidic devices are small, require minute sample volumes, and can be created in many forms, including those that maximize biologic to electronic information transfer (Shang et al., 2019; Vanarsdale et al., 2019; VanArsdale et al., 2022a; 2022b). In part, this is because the microenvironments they provide are steady and relatively easily controlled which makes them ideal operating platforms for sensing biomolecules in precious samples (Chen et al., 2023; Shang et al., 2019). They can be difficult to assemble and operate, however. We have created electrofabrication methodologies that enable simple, rapid assembly of biological components into devices (Liu et al., 2023). Importantly, these methodologies require no mechanical parts. Instead, electronic cues "program" assembly of stimuli responsive polymers, including those housing cells, proteins, and other biological materials (Li et al., 2021; Liu et al., 2023). Components are assembled directly onto electrodes precisely matching their spatial configuration. Moreover, the same electrodes are used for subsequent information transfer–in both directions–they can cue information to adjacent samples (i.e., actuate) as well as record information from the same samples (VanArsdale et al., 2020).

In this work, we created a "snap-in" 3D printed multichannel chip within which biomolecular sensing interfaces are assembled and utilized (Scheme 1a, center image). This chip is inserted into a 3D printed microfluidic housing that provides for simplified "plug and play" electronic connectivity. Here, we describe this sensor, its design, fabrication and use. The electroassembled thiolated polyethylene glycol (PEG)-based sensor captures mAbs based on their (1) Fc region and binding affinity to protein G, enabling assessment of antibody titer, and their (2) glycan pattern and binding affinity to lectins (Motabar et al., 2021). Unlike most traditional analytical chemistry methods, our sensing interfaces make use of biological molecular recognition elements and electrochemical sensing, enabling a direct molecular to electronic communication system. In our

previous report (Motabar et al., 2021), sensing interfaces were established on commercially acquired gold working electrodes and the assembly methodology, while simple, relied on manual, step-by-step interface construction, sample preparation, and finally, sample measurement. Because of the many steps, manual labor, sampling and washing protocols, operational errors were at times, unavoidable. Moreover, while simple, the step-by-step methodology was somewhat laborious.

To offer rapid, robust, and especially high-throughput approaches for biopharmaceutical process monitoring and control purposes, we have transformed the previous step-by-step methodology into an integrated automated platform wherein 8 parallel measurements are provided in near real time.

That is, we created an integrated platform that is based on our previously published protocol (Motabar et al., 2021) (Scheme 1a, bottom panel). We make use of a thiolated 4-arm polyethylene glycol (denoted PEG-SH) as a basis for functionalization and subsequent information transfer. PEG-SH is electroassembled onto a gold sensing surface by redox cycling of the mediator, 1,1′-Ferrocenedimethanol (Fc) and the electronic "activation" of sulfhydryl groups (to sulfenic acid) on the PEG. In turn, resultant sulfenic acid ($-SOH$) residues spontaneously link with adjacent free PEG thiols creating disulfide bonds and a film or gel directly associated with the electrode and its spatial configuration. That is, by applying an oxidizing voltage to an electrode immersed in a solution of the thiolated PEG and Fc (Li et al., 2020), we create disulfide bonds among the arms of the PEG creating a film or gel. Continued charging of the remaining sulfhydryl groups can then enable disulfide linkages with engineered recognition elements containing free thiols that are incubated with the film. This provides for selective capture of subsequently applied analytes. For the titer detection interface, we expressed and purified a cysteine-tagged protein G engineered to serve as the capture element (Motabar et al., 2021). Protein G was chosen because it enables the capture of IgG by binding its Fc region (Chames et al., 2009; Lund et al., 2011). After capture and subsequent incubation with an engineered reporter protein (a fusion of protein G and horseradish peroxidase ProteinG:HRP (Motabar et al., 2021; Motabar et al., 2023)) a sandwich assembly is created for detection (Scheme 1a, bottom right panel). In this way, the electrochemical outputs arising from the electron transfer mechanism between horseradish peroxidase (HRP), redox mediator 1,1′ ferrocenedimethanol (Fc), and hydrogen peroxide (H_2O_2) represent the analyte content captured on the interface. Analogously, for the glycan analysis, a galactosylation detection interface is created as a lectin model using a galactose-recognizing lectin, *ricinus communis agglutinin I* (RCA120), as the recognition element. RCA120 allows selective capture of antibodies with terminal β-galactose (Galβ) glycans based on traditional lectin-glycan binding (Itakura et al., 2007; Wu et al., 2006). Importantly, RCA120 is bivalent, meaning it can bind to a galactose covalently attached to the PEG as well as a galactose on the subsequently captured antibody. That is, a thiolated galactose is first conjugated to the PEG hydrogel using the Fc-based activation of the PEG thiols, exactly analogously as the assembly of the PEG. This
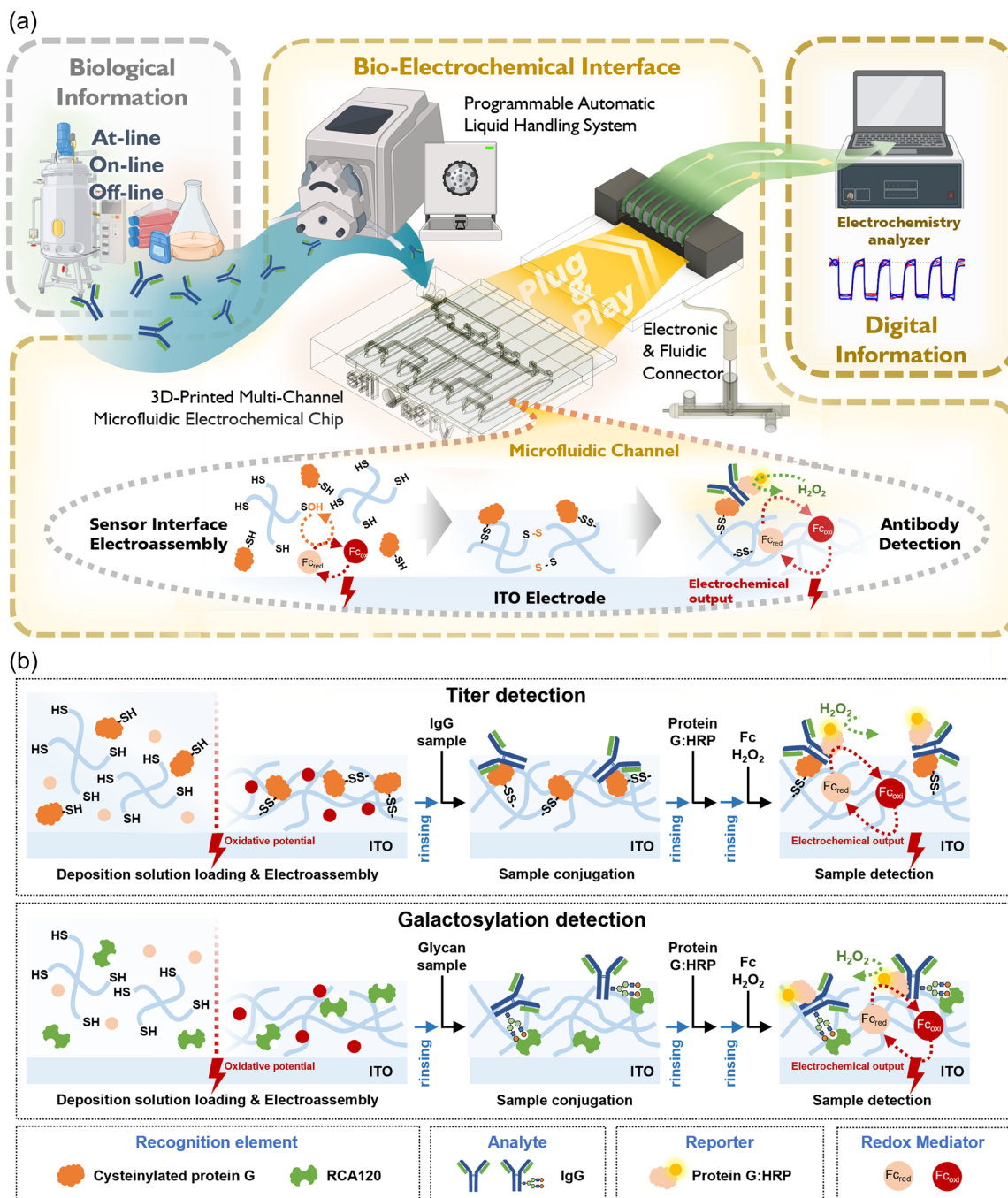
SCHEME 1 Schematic of modular antibody titer and glycan detection system. (a) The 3D-printed microfluidic device comprising eight parallel channels with transparent indium tin oxide (ITO) electrode and its affiliated modules (programmable automatic liquid handling system, and electronic & fluidic connector) is suitable for high-throughput detection of titer and glycan quality. The electroassembly of the sensor interfaces within the microfluidic "chip" is based on the oxidation of thiolated PEG. A typical sandwich structure (lower right) includes the recognition elements (protein G, brown cloud), analytes (mAb) and the reporter components (Fc, H_2O_2). Here, horseradish peroxidase (HRP, yellow circle) converts the hydrogen peroxide into water and oxidizes mediator Fc. The redox cycling process between the Fc and the electrode generates the electrochemical currents that report the analyte content on the interface. In this way, biological information (mAb concentration) then is recorded and converted directly into electrical signals that can be read and processed into digital signatures via the electrochemical analyzer. (b) Electrobiofabrication, functionalization, and sample detection of PEG sensor interfaces. Titer detection (upper panel) – deposition solution containing cysteinylated protein G, Fc, and PEG-SH is introduced into the channel. A brief (~1 min) oxidizing potential is provided for electroassembly followed by a short (~10 min) rinse. Samples with IgG are loaded, followed by another brief rinse. Then, reporter fusion protein:HRP is applied and rinsed. Finally, quantification is enabled by introduction of ferrocene and hydrogen peroxide to the HRP. Oxidized ferrocene is reduced at the electrode, where it cycles and amplifies the electronic signal. Galactosylation detection (lower panel)–deposition solution containing lectin RCA120, Fc, and PEG-SH is introduced into the channel. A brief (~1 min) oxidizing potential is provided for electroassembly followed by a short (~10 min) rinse. The sensing protocol after lectin capture is identical to the protein G capture in the upper panel.

places a galactose on the surface for subsequent assembly of the bivalent lectin. In turn, the lectin serves to capture the antibody in a sample solution.

To demonstrate transition to a fluidic system for subsequent mAb detection and quantification, we show the process workflow in Scheme 1b. Here, we combined PEG formation with the interface functionalization steps noted above by preparing one deposition solution containing thiolated PEG, Fc, and the recognition/capture elements (Titer detection, upper panel; Glycan detection, lower panel). That is, the disulfide linkages between thiolated PEG monomers and engineered cysteine residues of the protein G can spontaneously form along with the hydrogel crosslinking upon electro-deposition. Conversely, for the lectin assembly, we omitted the thiolated galactose and tested whether the lectin could be captured via the PEG crosslinking. Compared to our previous work, we reduced the rinsing and incubation times (to 10 and 30 min, respectively) for the mAb capture and protein G:HRP conjugation steps. We also rinsed once as compared to rinsing and washing three times previously. As noted above, the chip contains eight parallel channels for eight simultaneous measurements, which could include four of a sample and four of a control, or any combination thereof. As a result, the multichannel 3D-printed device reduces complexity, provides more data, and addresses an unmet need for implementation and operation in the biopharmaceuticals industry.

2 | RESULTS AND DISCUSSION

2.1 | System and device design, and fabrication

The streamlined sensing system is comprised of two major compartments: (1) a 3D printed "snap-in" chip that houses 8 parallel sensing channels, and (2) a 3D printed housing device with easy-to-use electrical connectors. The housing device also includes a fluidic controller for automation. As depicted in Figure 1a, the system features "plug-and-play" modularity which allows the user to quickly establish electrochemical bidirectional actuation and monitoring via the connected electrochemical analyzer. Meanwhile, the fluidic system is comprised of automated valves and a pump for precise sample operation. That is, the fluidic system employs two automated valves and one peristaltic pump for managing the 11 steps (Supporting Information S1: Table S1) required for sensor interface fabrication and sample detection (valve and flow diagrams are shown in Supporting Information S1: Figure S1). The first valve (valve A) is a 6-port selection valve, controlling the reagents (ethanol, water, 100 mM potassium phosphate buffer, 0.05% Tween-20 in 100 mM potassium phosphate buffer, 0.5 mM Fc in 100 mM potassium, and 0.5 mM Fc with 100 μM hydrogen peroxide in 100 mM potassium phosphate buffer). The second valve (valve B) is a 2-way 4-port valve managing the sample injection for (1) the deposition solution containing the interface and sensing components (i.e., thiolated PEG, cys-tagged protein G, thiolated galactose and lectin RCA120), (2) the sample with IgG, and (3) the reporting ProteinG:HRP fusion. As shown in

Figure 1b, this modular design facilitates use by automating device switching, reagent replacement, and system operation including data acquisition.

As the core compartment of the sensing system, the 3D printed microfluidic "chip" consists of eight ITO working electrodes, a shared reference electrode and a share platinum counter electrode. This constitutes the electronic sensor interface (Figure 2a). Taken together, this 3-electrode setup creates a stable environment for the thiolated PEG assembly. The microfluidic chip is comprised of two main components that are fabricated separately and then fused: (1) the 3D printed housing and (2) transparent ITO bottom electrodes. Its fabrication and assembly are illustrated in the upper panel of Figure 2a. As noted above, we selected ITO as the working electrode material (denoted "WE") due to its favorable conductivity relative to gold and other substrates, as well as its compatibility with optical signals (i.e., transparency). The 3D-printed housing consists of eight individual fluidic channels that are printed for parallel use. They have openings at the bottom, as well as sample inlets and outlets on the sides of the device. Symmetric splitting of fluidic pathways enables an even distribution of the samples among the eight chambers. After aligning the chambers with the ITO glass chip (that was laser engraved into eight parallel sub electrodes), we annealed the 3D printed housing to the glass by applying the identical 3D printing resin that comprises the chip, but at the boundaries of the two subsystems and exposing UV for 10 s. This seals the openings of the fluidic chambers, preventing subsequent leakage, and creates the eight parallel fluidic interfaces for electrochemical application. We note that the dimensions of the channels define the functional area of the bottom ITO working electrode (l × w × h: 13 mm × 1.5 mm × 200 μm, area: 27.924 mm^2) onto which the sensor elements are assembled.

To complete the three-electrode setup, we created a separate fluidic connector for the reference and counter electrodes. This fluidic connector contains five openings which, from left to right, accommodate the counter electrode, the potassium chloride solution, the reference electrode, and fluidic inlets and outlets (lower panel of Figure 2a). A 1 M KCl solution filling the fluidic connector enables ionic transport and conduction for electrochemical reactions while ensuring fluidic connection for the immersed counter and reference electrodes. Fresh KCl solution was fed to the fluidic connector at a flow rate of 200 μL/min. This flow minimizes mixing with the liquid samples introduced from the fluid inlet. The liquid sample from the microfluidic device enters the fluidic connector via the fluid inlet where it encounters the KCl solution entering from the left. The two fluidic flows intertwine at the junction on the right side of the fluidic connector and exit the system together from the fluid outlet. Consequently, this establishes a complete fluidic pathway starting from the sample inlet on the microfluidic chip and ending at the fluid outlet on the fluidic connector. Then, one can visualize the overall system that allows for interface assembly as well as the subsequent sensing via HRP and added hydrogen peroxide.

To complete the system, we created an electronics I/O system to enable access to the electrochemical capabilities of the microfluidic device. As illustrated in Figure 2b, we designed an electronics I/O
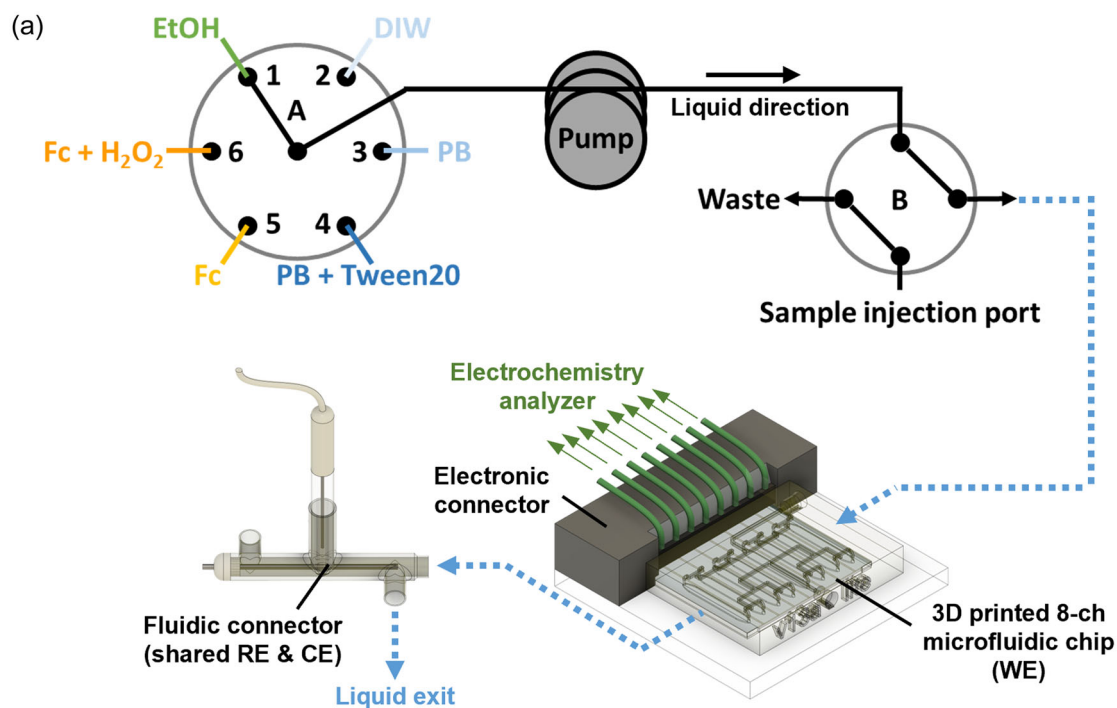
FIGURE 1 System design. (a) The system features two automated valves and a pump to enable fluid control. Reagents or samples are opened for entry via valve A (selection valve) and are pushed into the microfluidic sensor device via valve B (sample injection valve) and then into the fluidic connector to complete the electrochemical circuit. Finally, liquids exit the system from the outlet of the fluidic connector. (b) The images included on the leftmost side depict the chip in several configurations (held by fingers, next to the snap in housing (electronic connector), and as wired). At the right, the chip containing all fluidic sensing channels (1) is "snapped" into a 3D-printed electronic connector which establishes the signal pathways towards the electrochemical analyzer (2). The chip is also connected to a fluidic connector (3) which enables stable fluidic transport between all working, counter, and reference electrodes. The valves (5) served to partition reagents, buffers, and samples wherein they are flowed through the device by the pump (4).
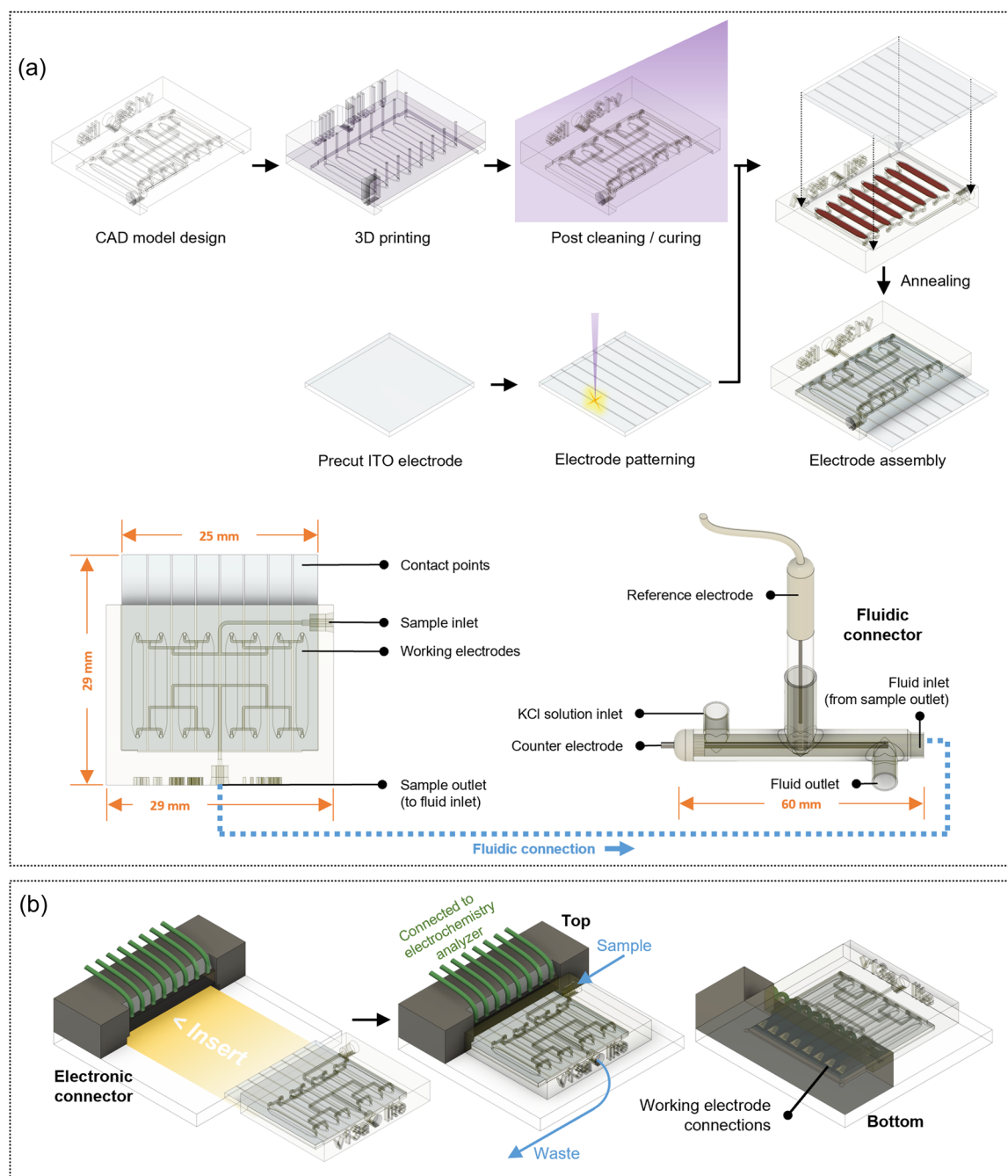
FIGURE 2 ITO microfluidic device assembly and affiliated connectors. (a) The eight parallel ITO electrodes on the glass substrate align with the 8 channels on the 3D printed device. When bonded together, they together form eight individual electrochemistry ready channels for sensor interface fabrication. The fluidic connector comprises the reference electrode and counter electrode and fluidically connects the microfluidic module which enables transport for chemical reactions. (b) The electrical connector provides a "plug-and-play" modularity for the 3D printed microfluidic systems and makes it straightforward when the users need to quickly switch between functional modules.

connector so that it is easily employed, utilizing a "snap-in" configuration. This avoids the more common alligator clip designs that are less well connected and easily moved/disconnected at the wrong times. Here, our design features two 4-way spring connectors, providing a total of eight connection points for parallel data transfer with the eight test channels already assembled and fused. In conjunction with the fluidic connector, the working electrodes, counter, and reference electrodes form eight complete circuits for electrochemical reactions. The ITO teeth of the microfluidic device are inserted into the slot on the connector, establishing an instant connection via spring metal pins. This "plug-and-play" design enables rapid device replacement and module switching, ultimately facilitating high-throughput, multi-sample detection. As noted, this connector serves as an interface, linking the ITO device to a programmable potentiostat that controls the entire system.

2.2 | Channel uniformity and fluidic performance

Fluidic uniformity and stability are likely channel dependent, and their quality further determines system robustness and measurement reproducibility. In initial studies, we utilized both a simulation tool and actual fluidic examinations (electrochemical measurement of Fc solutions) to determine the flow uniformity and fluidic performance. Specifically, we developed a 3D model of the device using the Laminar Flow module of commercially available COMSOL Multiphysics software for visualization and prediction of the fluidic patterns at various locations and flowrates (Figure 3a). First, we calculated that a flow rate of 1 mL/min for the sample flow (and assembly/wash flows) could best suit our desire for rapid transport, film assembly, reagent incubation, etc, and we used this flow rate in all subsequent experiments. As illustrated Figure 3b (top), our computational design provides for symmetric fluidic distribution to the channels; we predicted an even distribution of the liquid sample into the eight parallel detection channels. Then, these separate flows were then merged into one combined flow exiting the system from the outlet at the top. In our in silico test conditions, a color indicator provided for a visualized flow pattern which made evaluation simple. Color uniformity (Figure 3b) suggests that fluidic resistance was properly distributed within each channel. Then, to estimate representative flow patterns *within* the detection channels (with assembled detection interfaces), we simulated the flow velocities at a focal plane 50 μm above the bottom electrode (the surface of a PEG interface, Figure 3b [bottom]). Our results indicated that when liquid samples entered the middle sections of each channel, the flow velocity remained consistent across all eight channels.

Next, we evaluated the fluidic performance by examining electrochemical reactions and corresponding electrical signals (Figure 3c). We prepared a 100 mM phosphate buffer (PB) solution (negative control) and a 100 mM PB solution containing 100 μM of Fc (positive control), infusing each test solution into the microfluidic device for 60 s at a flow rate of 1 mL/min. We repeated the process five times. During these tests, we continuously applied an oxidative potential of 0.4 V to all working electrodes and measured the current on each. That is, Fc is oxidized at the electrode generating a corresponding current when there is an applied voltage. As anticipated, we observed minimal currents during an infusion stage with PB (no redox mediator), while significant currents were detected during Fc infusion (top panel of Figure 3c). Both the dynamic data and averaged data from the last 30 s of each period are depicted (middle panel of Figure 3c). These are representative of the general performance over many such tests of the combined fluidic, electrochemical, and instrumentation systems. Notably, the overall assembly seemed quite robust. The measurements were steady, and all 8 channels give similar amplitudes and dynamic responses. Meanwhile, it is also noteworthy that at a flow rate of 1 mL/min, the recorded signal demonstrates that a rapid response from the electrode is feasible, with the current change detected and equilibrium established within 2 s after a fluidic switch. This rapid response is a well-known advantage of microfluidic systems. As illustrated in the detail of the middle panel of Figure 3c, our

device exhibited promising electrochemical results, showing a high degree correlation and alignment with the simulation results. Finally, because responses from the electrochemical reactions should depend on the mediator concentration, we prepared Fc solutions with varying concentration (5, 10, 25, and 100 μM) and evaluated the corresponding Fc signals again at a flow rate of 1 mL/min. Following the same testing procedures, we found there was minimal difference in measured current between 25 and 100 μM of Fc, but currents decreased with further decreasing concentrations, as expected. These provided design data for subsequent mAb sensing.

Overall, these studies showed that the ITO microfluidic device, its associated fluidic system, and electrochemical analyzing capabilities, were robust, reproducible, and rapid. Moreover, because of the snap-in or plug and play designs, we anticipated excellent utility in subsequent antibody measurements.

2.3 | Electroassembly of thiolated PEG-based sensor interfaces

To streamline the system for parallel and automated use, we first recapitulated the steps previously described for the formation of the sensor interfaces for target IgG detection but within our device (Figure 4a). First, the deposition solution (a mixture of 25 mM of Fc, 50 mg/mL of thiolated-PEG, and 250 μg/mL of C-terminus cysteine tagged protein G prepared in 0.1 M PB, pH 7.4) was added to wet the ITO electrode. Interface electrodeposition occurred for 1 min at a constant oxidative potential of 0.8 V. Solutions containing 62.5 mg/L of IgG and 0.1 g/L of protein G:HRP were also separately prepared for the final assembly. Wash buffer (0.05% Tween-20 in 0.1 M PB) was used for rinsing the hydrogel to remove unconjugated residues between steps. Next, we prepared mediator Fc solutions (0.5 mM) with and without peroxide (100 μM) for the electrochemical output tests. We note that the HRP on the reporter protein G ultimately converts the peroxide in the solution into redox-active radicals, leading to Fc oxidation. By applying a potential of 0 V on the electrode, we record the redox signals of Fc in the form of current. As shown in Figure 4b, we initially infused the Fc solution at a flow rate of 1 mL/min to record the system's blank signals. We later used this data to define the sensitivity of this interface. After 30 s, we switched the valve and introduced Fc solution containing peroxide, resulting in an instantaneous current spike (3 s). After a series of tests with IgG, we found that the current spike corresponded to the total amount of reporter protein G:HRP conjugated to the analyte IgG. Most importantly, there was substantial uniformity across the 8 electrodes.

That is, in additional experiments, we switched the valve and repeatedly infused the Fc solution to monitor the interface's response time. The current consistently returned to its initial level within 20 s after an infusion of peroxide was stopped. This indicated that the response time of the measurement was both quick, but was also terminated quickly, potentially enabling reuse. Upon repeated cycling we found subsequent measurements ($n = 8$) were typically within 93% of the original responses. Then (Figure 4b), current data from the last 7.5 s of each
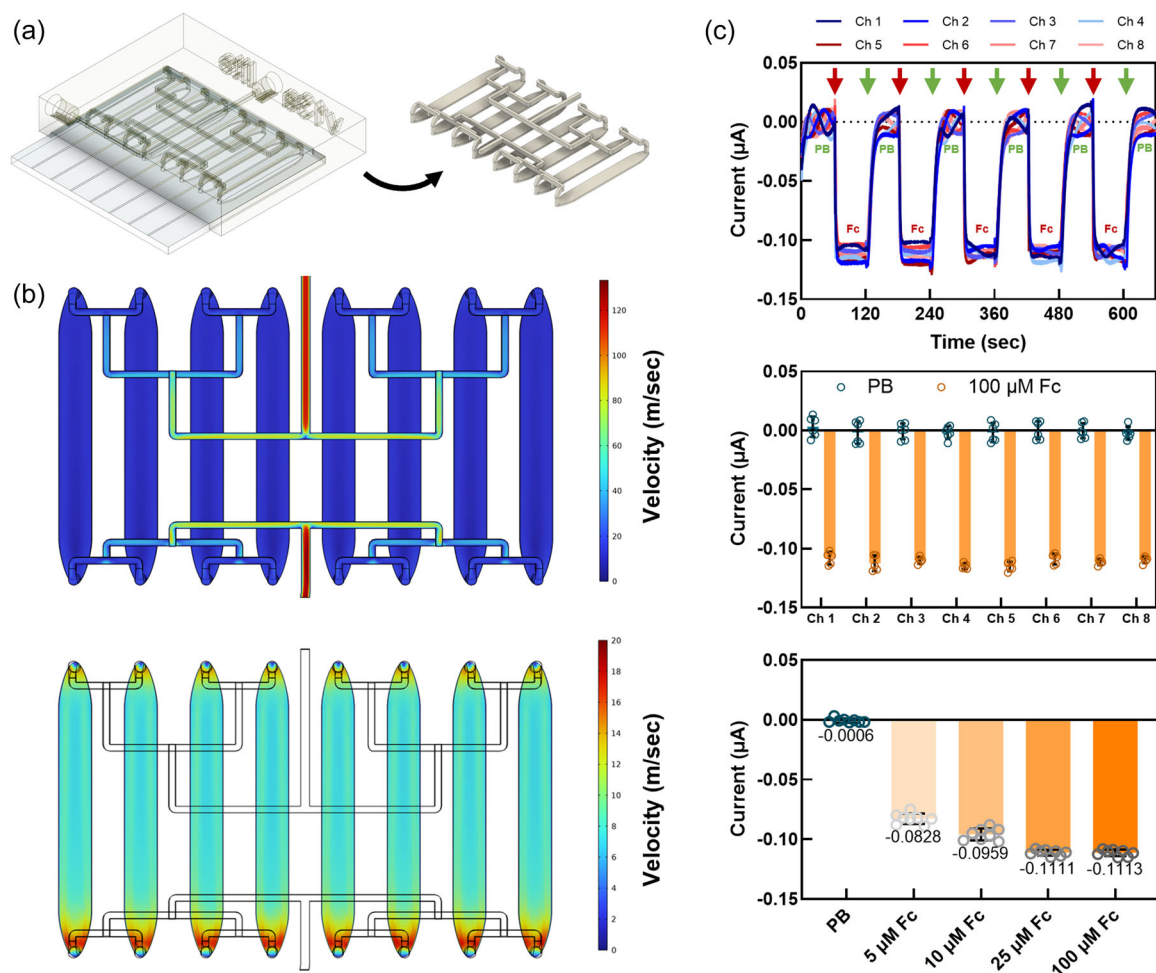
FIGURE 3 Simulation and fluid uniformity testing using redox mediator 1,1 -Ferrocenedimethanol. (a) The 3D model for COMSOL simulation was generated directly from the original device model. (b) The top panel demonstrates that the infused fluidic sample can be distributed across all parallel channels and then merged at the exit. The bottom figure displays the predicted flow velocity 50 μm above the bottom ITO electrode, illustrating uniformity in flow within the channels. (c) The currents measured during repeated infusion between the PB solution and the Fc solution confirm rapid dynamic response and robustness and reproducibility of the overall system. *(n = 8).

test period was collected and averaged, representing the general output of the system. Results were highly consistent among all channels. Also, as shown in Supporting Information S1: Table S2, the relative standard deviation (RSD) of individual electrodes with and without H_2O_2 was below 0.45% and 1.85%, respectively. The RSD of the blank test (Fc solution) and test group (sensing reagents, and 100 μM H_2O_2) across all eight electrodes was 2.53% and 3.56%, respectively. Together, these tests illustrate electroassembly of thiolated PEG-based sensor interfaces and that results previously obtained using sequential batch processing were now more rapid, parallel, and reproducible across independently-fabricated and functionalized electrodes.

2.4 | Detection of antibody titer and galactosylation

We next assessed the capability of the protein G recognition interface to capture and detect IgG at various IgG concentrations. As

illustrated in the left panel of Figure 5a, we employed a one-step deposition strategy to construct the recognition interface. After the system conditioning steps, the deposition solution (a mixture of 25 mM of Fc, 50 mg/mL of thiolated-PEG, and 250 μg/mL of C-terminus cysteine-tagged protein G prepared in 0.1 M PB, pH 7.4) was loaded, followed by electrodeposition for 1 min at a constant oxidative potential of 0.8 V. The valve was switched, rinsing the interface with the wash buffer. Varying concentrations (0.0001, 0.001, 0.002, 0.01,0.02, 0.1, 0.2 mg/L) of human IgG samples were prepared and infused into several microfluidic devices where they were incubated for 30 min. Interfaces were washed for 10 min, the reporter protein G:HRP was then infused so that when bound to the analyte mAb, it forms the sandwich structure that is then quantified electrochemically via H_2O_2 and Fc. We infused an Fc solution for 1 min for system equilibration. With the solution still flowing, we applied an open circuit potential (0 V) for signal recording. For the first 30 s, we recorded the "Off" current (baseline) of the system. We then infused Fc solution containing H_2O_2 for another 30 s which is
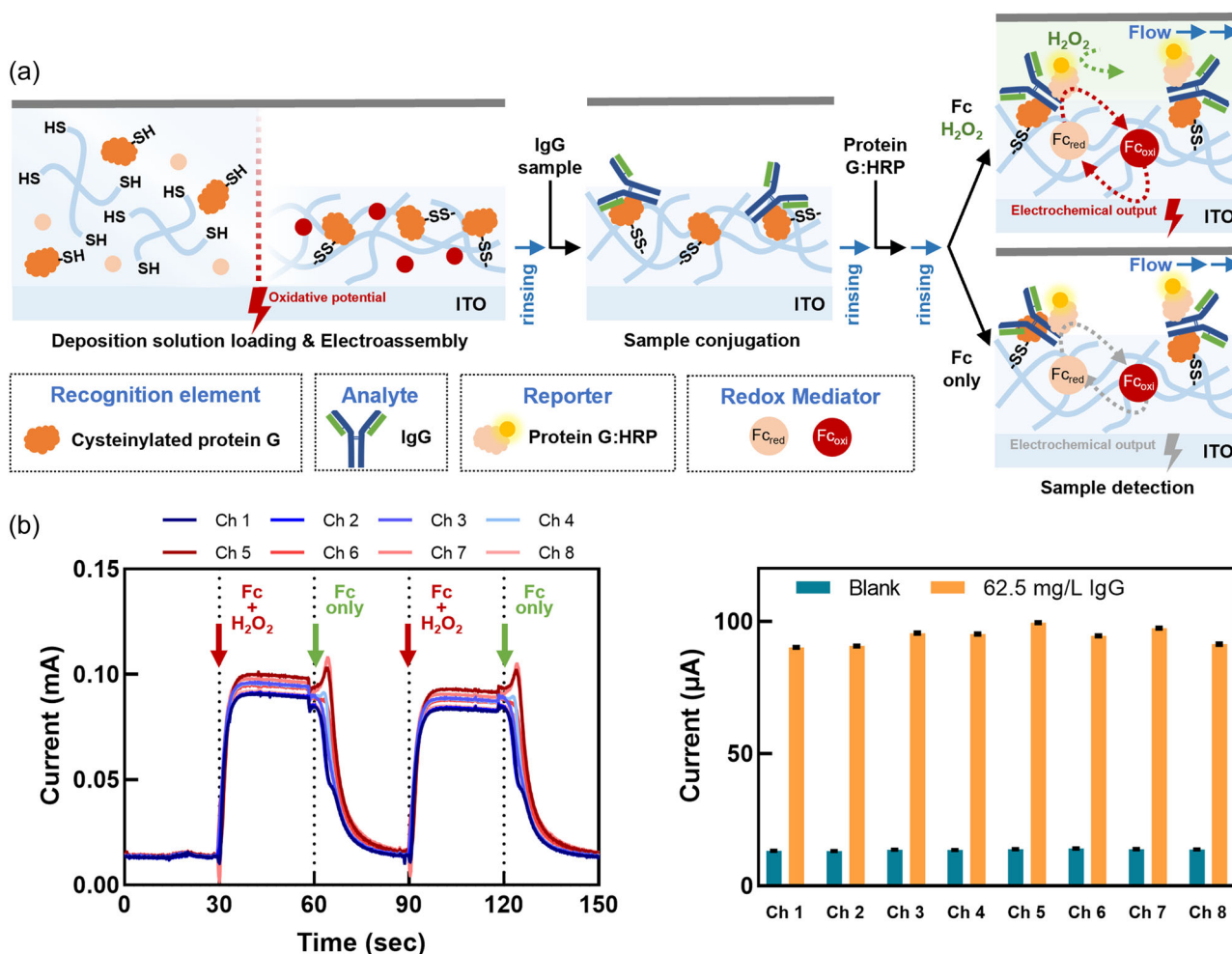
FIGURE 4 Electroassembly, dynamic response time, and reproducibility of sensor interfaces. (a) Schematic representation of the electroassembly of thiolated PEG-based sensor interfaces. Three major steps are required for the IgG detection: (1) electroassembly of the PEG recognition region, (2) sample conjugation, (3) reporter protein G:HRP conjugation. Rinsing (10 min) was required to eliminate nonspecific binding between each steps. (b) left panel: After functionalizing surfaces, loading mAb test solution (62.5 mg/L), and then reagent solutions, current data for two cycles of PB-H_2O_2 infusion are depicted. Data for all eight electrodes indicate high reproducibility and robustness of hydrogel and interface formation. (b) right panel: The signals with IgG, proteinG:HRP, Fc, and H_2O_2 show significant differences from the blank. Minimal deviation across the electrodes also indicates uniformity of the fluidic and electronics subsystems. *(n = 8).

recorded as the "On" current of the test condition. The current reached equilibrium within 5 s, almost exactly as in Figure 4. The calculated difference between the "Off" and "On" currents served as the net signal for the assembled IgG (cysteine-tagged protein G-IgG-protein G:HRP, Figure 5b). After conducting a series of tests at various IgG concentrations, we found that the measured currents corresponded well to the total amounts of sandwich conjugations. To evaluate robustness and reproducibility, we cycled between PB-Fc and PB-Fc-H_2O_2 and have depicted the first and second measurements (reused identical surface with new IgG test solution) across all channel responses and found they were rapid, consistent, and reproducible. The responses relative to their IgG concentration were then modeled using a Langmuir isotherm, and a double-reciprocal plot ($R^2 = 0.99$). We found a linear response (double-reciprocal plot) for IgG concentrations up to ~0.2 mg/L.

Similarly, we evaluated the capability of the RCA120 recognition interface to IgG galactosylation. Note that we follow the same operating conditions (test sample concentrations, incubation time, wash time, flow rate, and electrochemical recording setup) as described for titer detection. Here, we used RCA120 as the recognition element instead of the C-terminus cysteine-tagged protein G. In Figure 5a, we once again used the one-step deposition strategy to construct the PEG network with RCA120 recognition elements. The deposition solution (500 μg/mL of RCA120) was loaded for 2 s (100 μL) then stopped, followed by electrodeposition for 1 min at a constant oxidative potential of 0.8 V. After testing varying concentrations (0.0001, 0.001, 0.002, 0.01,0.02, 0.1, 0.2 mg/L) of human IgG samples, we observed that the overall current responses were remarkably consistent and reproducible (Figure 5c). Interestingly, while there should be no obvious reason that lectin- and
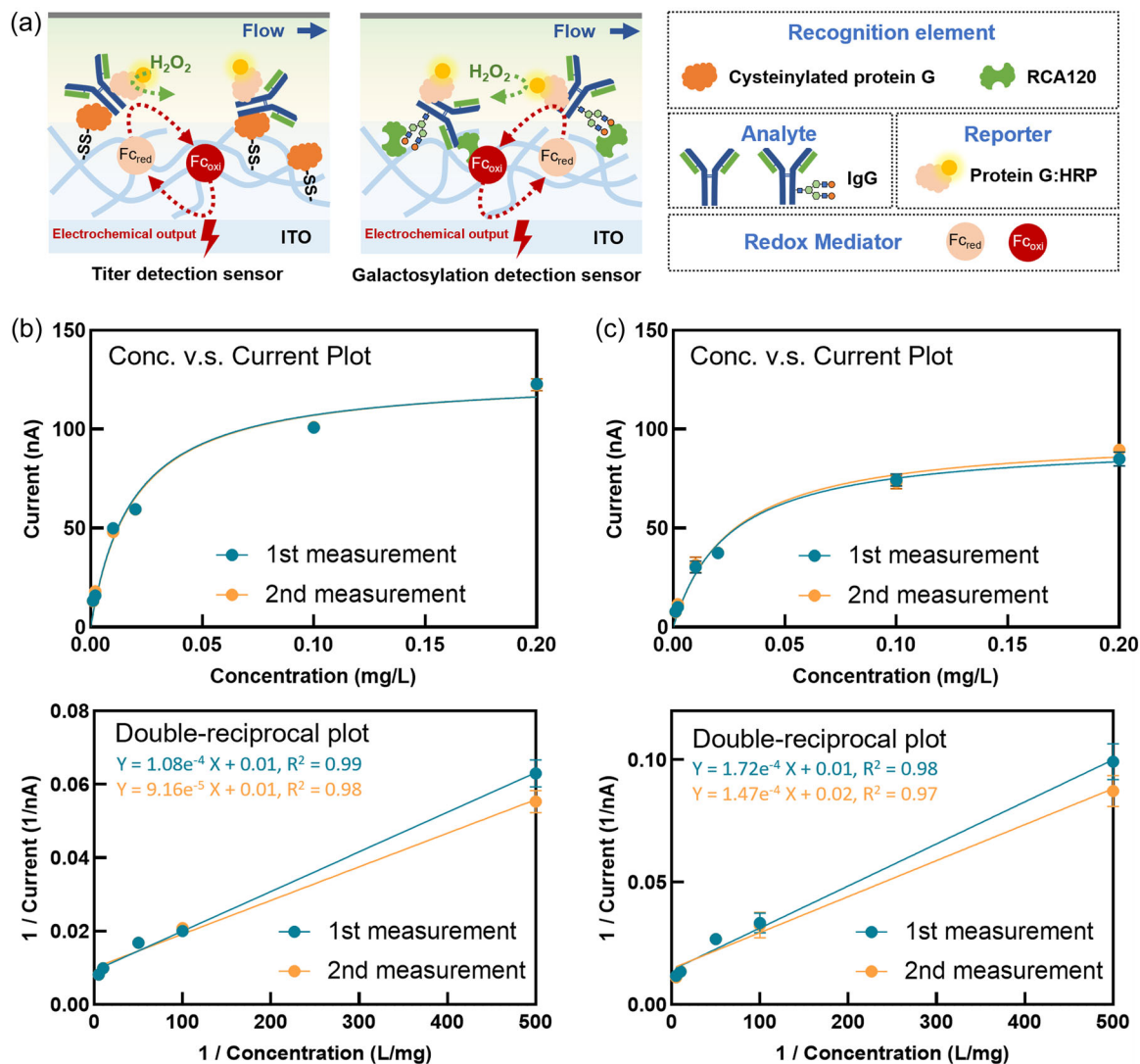
FIGURE 5 Quantification of antibody titer and galactosylation using detection system. (a) Schematic (top) depicts the interfaces that facilitate titer and galactosylation measurements in the microfluidic device. (b) Titer measurements taken with IgG (concentrations of 0.0001, 0.001, 0.002, 0.01,0.02, 0.1, 0.2 mg/L) and protein G: HRP (100 mg/L) with the integrated microfluidic housing and the titer detection interface. Current responses from channels are consistent, rapid, and reproducible. Averaged responses were fit using a Langmuir isotherm model and double-reciprocal plot. (c) Glycan measurements taken with IgG (concentrations of 0.0001, 0.001, 0.002, 0.01,0.02, 0.1, 0.2 mg/L) and protein G: HRP (100 mg/L) with the integrated microfluidic housing and the antibody galactosylation detection interface. Current responses from channels are consistent, rapid, and reproducible. Averaged responses were fit with a Langmuir isotherm model and double-reciprocal plot. *($n = 8$).

proteinG-based binding should enable the same, or close to, mAb binding capacity, the currents achieved were similar. That the currents are significant (>10 nA) indicates that the electrode surfaces and miniscule levels of reagents were sufficient for accurate quantification. Importantly, the IgG concentrations using lectin binding were also found to follow a Langmuir isotherm and were plotted using a double reciprocal plot ($R^2 = 0.98$). Similarly, the linear range on the double reciprocal plot suggested accurate measurements up to 0.2 mg/L. In our previous work, we showed that IgG results taken from solutions of both new and spent media were consistent. Instead of a complete analysis here, we show in Supporting Information S1: Figure S2 that currents from PB and fresh culture media were similar

at 62.5 mg/L. Thus, while we have not analyzed fully the different backgrounds when interfaces are assembled in a device, we expect similar transitions from large electrodes to small devices will be repeated (smaller samples, smaller but measurable currents, etc).

In sum, our demonstrated results show that both sensor interfaces (for antibody titer and lectin binding galactosylation) can be electroassembled onto ITO electrodes within the same 3D printed microfluidic device using the identical assembly methodology. When combined with the fluidic system and automated valving and pumps, we noted that the systemic variations were quite small, varying from 1.9% to 6.8%. These results suggest significant potential for high-throughput and reliable measurements in bioprocessing settings.

2.5 | Regeneration of interfaces

We decided to try to strip the surface, regenerate, and reassemble onto the same thiolated PEG hydrogel films to reassess the titer measurements. That is, a low pH regeneration buffer containing 0.1 M acetic acid and 1 M sodium chloride, pH 2.8, was found to decouple the protein-antibody interactions on our previous batch systems using gold electrodes. This regeneration buffer had removed the conjugated IgG while keeping the cysteinylated protein G (for the titer detection interface) that was covalently coupled onto the PEG using electronically oxidized disulfide bonds. Here, we evaluated the same regeneration process for the current interface situated atop the ITO electrodes. In Figure 6a, we infused the regeneration buffer into the microfluidic device at a flow rate of 0.5 mL/min for 10 min. This was followed by a rinsing buffer to remove acidic residues at the same flow rate for 10 min. The interfaces were then sequentially incubated with IgG sample solution and protein G:HRP solution, and repeated measurements were taken following the previously described protocol. In Figure 6b, we compared three conditions (no IgG, 62.5 mg/mL of IgG, and 250 mg/mL of IgG). We found that the electrochemical responses for the control (no IgG but after regeneration) were completely diminished, suggesting that the IgG and the reporter protein G:HRP were decoupled and removed from the system. After reconjugating the analyte IgG and protein G:HRP, we observed that the signal strengths from the second conjugation were nearly identical to the original measurements. These results suggest that the interfaces containing the recognition elements remained intact and were essentially unaltered after the acidic decoupling process. They were still able to maintain their initial capturing capability without significant loss of activity. As noted above, we did complete a full regeneration analysis of the lectin-based interface.

3 | CONCLUSIONS

We describe the development and testing of a 3D-printed microfluidic device for electrochemical interrogation of antibody titer and glycosylation. We designed and fabricated an 8-channel microfluidic device consisting of ITO electrodes that are subsequently electrochemically functionalized for IgG capture and measurement. The devices have affiliated fluidic and electrical connector subsystems that are also 3D-printed. We found that 3D printed housings and channels were sufficient for generating the fluidic routes, such as splitting fluidic pathways, flowing fluids through electrode channels, and then reassembling flows to waste streams. The designs were first evaluated numerically using 3D COMSOL simulations that quantitatively examine the flow patterns across all test channels. Simulation results were shown to be highly correlated with subsequent fluidic test results. Equally important, by introducing an automated valving and fluidic transfer system, we were able to show precise fluidic control among 8 parallel channels and this significantly reduced labor and manual processing otherwise required for operation. As a result, this also led to substantial enhancements in signal consistency,

reproducibility, and reliability. We also showed that the "plug-and-play" modularity provides for rapid device replacement and module switching, which could potentially offer solutions for multi-sample quality assessment during biopharmaceuticals production.

We subsequently demonstrated that the microfluidic system was amenable for integration with an electroassembled thiolated PEG-based antibody detection interface. Specifically, we showed that the recognition elements could be constructed in a single, one-pot assembly step, and the analyte and reporter proteins could be successfully conjugated to the parallel interfaces. The integrated device was shown to reliably quantify a range of IgG concentrations. We further found that the sensing interfaces could be regenerated and re-probed, which suggests further utility. While the glycan assessment here is based on targeting galactosylation, there is no reason to expect one could not establish several different channels for different lectins, enabling a signature type of reporting approach. In sum, we believe rapid assessment of both antibody titer and galactosylation can facilitate a researcher's decision-making process for establishing conditions that improve product quality and consistency. Because a feature of this system is that it provides direct quantitative electronic outputs, we suggest that it could be incorporated into a process controller wherein corrective actions could be taken in real time.

4 | METHODS

4.1 | Materials

Square indium tin oxide coated glass slides (surface resistivity 8–12 Ω/sq) were purchased from Sigma. RCA120 and fluorescein labelled conjugate (FITC RCA120) were purchased from Vector Laboratories. IgG from human serum, SILU Lite SigmaMAb, and protein G:HRP conjugate and phosphate buffered saline (PBS, pH 7.4) were purchased from Sigma-Aldrich (St. Louis, MO). Clear 3D microfluidics printing resin was purchased from CADworks3D (Toronto, Canada). 1,1′-Ferrocenedimethanol (Fc) was purchased from Santa Cruz Biotechnology. A 1 M stock solution of Fc was prepared in DMSO, and dilutions were prepared in PBS freshly for each experiment. Dulbecco's Modified Eagle medium, high glucose, HEPES, no phenol red (DMEM) was purchased from Thermo Fisher Scientific.

4.2 | Device fabrication and performance assessment

The 3D printed eight-channel microfluidics device with ITO electrodes was designed based on a standard 3-electrode system including a device with 25 mm × 25 mm ITO working electrode (split into eight sub working electrodes), and an electrical connector that allows wiring to an electrochemical analyzer (CHI multichannel potentiostat). A Pt wire serves as the counter electrode and an Ag/AgCl reference electrode connects to the device via a fluidic connector. To make the 3D printed device housing, designs were created using
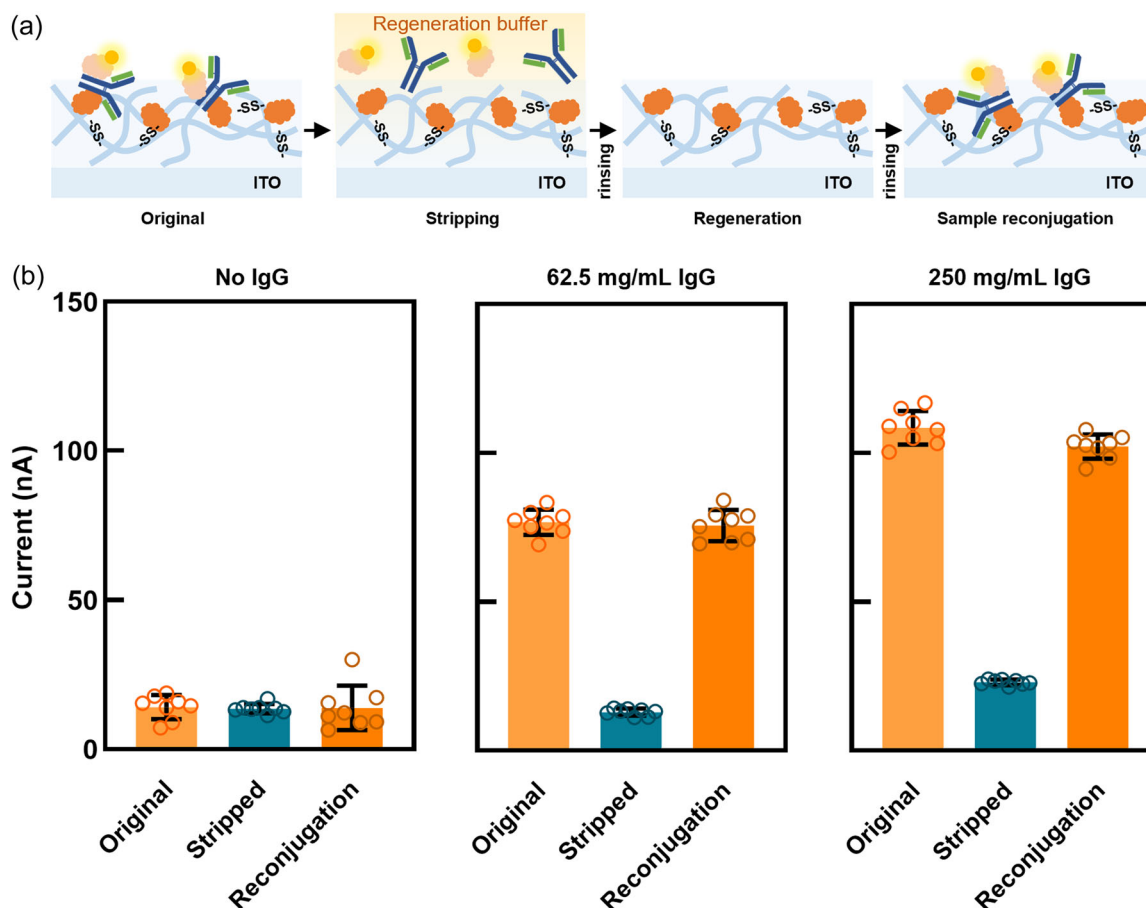
FIGURE 6 Regeneration of titer interfaces. (a) Schematic representation of the regeneration process. The initial protein-antibody conjugation is decoupled by introducing a low pH regeneration buffer. The cartoon suggests the proteinG recognition element is retained within the PEG for subsequent IgG measurements. (b) The original, stripped and final currents after assembly are depicted for several IgG concentrations. In all cases, the currents after regeneration buffer were similar to the zero IgG samples, as expected. Then, currents after capture and sandwich reporting assembly were similar to the original signals suggesting the capture and subsequent wash and incubation steps were quite similar between runs. *($n = 8$).

Autodesk® Fusion 360 and Autodesk® Inventor (Autodesk, Inc). The CAD files were then converted to writing-path using the Chitubox 1.9.4. Mars 3 Pro was used to fabricate the housing. When the printing process was completed, the substrate was placed in a bath of methanol with gentle shaking by hand for 1 min and then dried with nitrogen. This step was repeated three times to thoroughly remove any uncured residues. The prints were then further cured under a 20-Watt UV lamp for 10 s followed by a 30-second rest at room temperature. This step was repeated three times to achieve full strength. Purchased precut ITO glass (25 mm × 25 mm) was patterned with a CO_2 laser engraver to physically define all electrodes and the connecting regions. The cured housing was then aligned with the laser patterned ITO glass and annealed together with the same photosensitive resin used for printing. The design and the fabrication of the electrical connector generally followed the same protocol described above. Two four-way spring connectors (Digi-Key, Part Number 478-4688-6-ND) were then attached to the designed location on the printed electrical connector in which later enabled the physical connection to the ITO device. The other end of the four-way spring connectors were soldered with wires to connect to the electrochemistry analyzer. The fluidic connector was made with a T-shape 3-way connector. The tubing was glued to the connector with epoxy resin.

For the simulation model: The numerical (finite element method) simulations for infusion-diffusion model were performed using the Laminar Flow module of commercially available COMSOL Multiphysics software (version 5.6). Geometry and fluidic setups were defined based on the dimensions and parameters provided previously. The fluidic conditions were described by Navier-Stokes equations.

For the fluidic test: Two test solutions were prepared: 100 mM phosphate buffer (PB) solution (negative) and a 100 mM PB solution containing 100 μM of 1,1′-Ferrocenedimethanol (Fc) (positive). They were connected to port No.1 and port No.3 of the 2-way 4-port valve and introduced using a flow rate of 1 mL/min. Each test solution was flowed into the microfluidic device for 60 s as one

independent cycle and the process repeated five times. Meanwhile, an oxidative potential of 0.4 V was applied to all working electrodes and currents were measured for each. Current data spanning the last 30 s of each run was collected and averaged for analysis. Followed the same protocol, solutions with varying Fc concentration (5, 10, 25, and 100 μM) were also tested.

4.3 | Titer and galactosylation detection interface measurements

Measurements of the current responses from the interfaces were performed with the 3-electrode set-up using a CHI1040C electrochemical analyzer (CH Instruments). For assembly of titer interfaces, a solution of Fc (25 mM), PEG thiol (50 mg/mL) and C-terminus cysteine tagged protein G (250 μg/mL in 0.1 M PB, pH 7.4 [Wang et al., 2021]) was prepared and injected (100 μL) into the microfluidic device (using the device injection port). Interface electrodeposition occurred for 1 min at a constant oxidative potential of 0.8 V. After electrodeposition, the peristaltic pump was activated and channels were rinsed with wash buffer (PBS, 0.05% Tween-20, pH 7.4) for 10 min at a flow rate of 0.5 mL/min (20 rpm coupled with black-black PVC tubing purchased from Gilson). The devices were then sequentially incubated in serially diluted concentrations of IgG (0–200 μg/L) and protein G:HRP (100 mg/L), respectively, at room temperature for 30 min. After each respective incubation (IgG and protein G:HRP), the channels were rinsed with wash buffer for 10 min at a flow rate of 0.5 mL/min. Current measurements were then performed using constant potential amperometry. Specifically, the devices were run under an applied potential of 0 V and Fc (0.5 mM) was pumped at a flow rate of 1 mL/min (20 rpm coupled with black-black PVC tubing purchased from Gilson) until a constant baseline was achieved. To generate a current response, the infused liquid sample was then switched to a solution of Fc (0.5 mM) and H_2O_2 (100 μM) and the response from baseline was recorded. The lower limits of detection for the titer detection interface were calculated as previously described (Motabar et al., 2021; Motabar et al., 2023). For construction of galactosylation interfaces on the microfluidic device, the C-terminus cysteine tagged protein G in the deposition solution was replaced with RCA120 (0.5 mg/mL in 0.1 M PBS, pH 7.4).

4.4 | Interface regeneration studies

To evaluate regeneration, the detection interfaces were assembled with IgG from human serum (1000 mg/L) and protein G:HRP (100 mg/L) and measurements of the current response were taken using the same conditions as above. The interfaces were then washed with 0.1 M acetic acid, 1 M sodium chloride, pH 2.8 at the flow rate of 0.5 mL/min to decouple IgG and protein G:HRP from the recognition elements on the surfaces, leaving only the capturing proteins (i.e., protein G) covalently bound to PEG. Current measurements were taken to confirm that IgG and protein G:HRP were removed. The

interfaces were once again re-assembled with IgG and protein G:HRP. Current measurements were taken to confirm the re-binding of IgG and protein G:HRP to the interface surfaces. In results not shown, we found refrigerated interfaces left unattended for ~7 days were fully functional.

CONFLICT OF INTEREST STATEMENT
The authors declare no conflict of interest.

DATA AVAILABILITY STATEMENT
The authors declare that the data supporting the findings of this study are available within the paper and its Supplementary Information file. If raw data files are needed in another format, they are available from the corresponding author upon request.

ORCID
Chen-Yu Chen http://orcid.org/0000-0001-6500-6970
William E. Bentley http://orcid.org/0000-0002-4855-7866

REFERENCES
Chames, P., Van Regenmortel, M., Weiss, E., & Baty, D. (2009). Therapeutic antibodies: Successes, limitations and hopes for the future. *British Journal of Pharmacology*, *157*(2), 220–233. https://doi.org/10.1111/J.1476-5381.2009.00190.X

Chen, Y.-S., Huang, C.-H., Pai, P.-C., Seo, J., & Lei, K. F. (2023). A review on microfluidics-based impedance biosensors. *Biosensors*, *13*(1), 83. https://www.mdpi.com/2079-6374/13/1/83

Gerzon, G., Sheng, Y., & Kirkitadze, M. (2022). Process analytical technologies – advances in bioprocess integration and future perspectives. *Journal of Pharmaceutical and Biomedical Analysis*, *207*, 114379. https://doi.org/10.1016/j.jpba.2021.114379

Itakura, Y., Nakamura-Tsuruta, S., Kominami, J., Sharon, N., Kasai, K., & Hirabayashi, J. (2007). Systematic comparison of oligosaccharide specificity of *Ricinus communis* agglutinin I and erythrina lectins: A search by frontal affinity chromatography. *Journal of Biochemistry*, *142*(4), 459–469. https://doi.org/10.1093/JB/MVM153

Langer, E., & Rader, R. (2015). Biopharmaceutical manufacturing: Historical and future trends in titers, yields, and efficiency in commercial-scale

bioprocessing. *BioProcessing Journal*, 13(4), 47–54. https://doi.org/10.12665/J134.LANGER

Li, J., Kim, E., Gray, K. M., Conrad, C., Tsao, C.-Y., Wang, S. P., Zong, G., Scarcelli, G., Stroka, K. M., Wang, L.-X., Bentley, W. E., Payne, G. F., & Wang, L. x (2020). Mediated electrochemistry to mimic biology's oxidative assembly of functional matrices. *Advanced Functional Materials*, 30(30), 2001776. https://doi.org/10.1002/ADFM.202001776

Li, J., Wang, S. P., Zong, G., Kim, E., Tsao, C.-Y., VanArsdale, E., Wang, L.-X., Bentley, W. E., & Payne, G. F. (2021). Interactive materials for bidirectional redox-based communication. *Advanced Materials*, 33(18), 2007758. https://doi.org/10.1002/ADMA.202007758

Liu, Y., Kim, E., Lei, M., Wu, S., Yan, K., Shen, J., Bentley, W. E., Shi, X., Qu, X., & Payne, G. F. (2023). Electro-biofabrication. Coupling electrochemical and biomolecular methods to create functional bio-based hydrogels. *Biomacromolecules*, 24(6), 2409–2432. https://doi.org/10.1021/acs.biomac.3c00132

Lund, L. N., Christensen, T., Toone, E., Houen, G., Staby, A., & St. Hilaire, P. M. (2011). Exploring variation in binding of protein A and protein G to immunoglobulin type G by isothermal titration calorimetry. *Journal of Molecular Recognition*, 24(6), 945–952. https://doi.org/10.1002/JMR.1140

Motabar, D., Kim, E., Li, J., Zhao, Z., Mouchahoir, T., Gallagher, D. T., Schiel, J. E., Garige, M., Sourbier, C., Payne, G. F., & Bentley, W. E. (2023). Detecting features of protein structure through their mediator-accessible redox activities. *bioRxiv*, 2023, 571363. https://doi.org/10.1101/2023.12.12.571363

Motabar, D., Li, J., Wang, S., Tsao, C. Y., Tong, X., Wang, L. X., Payne, G. F., & Bentley, W. E. (2021). Simple, rapidly electroassembled thiolated PEG-based sensor interfaces enable rapid interrogation of antibody titer and glycosylation. *Biotechnology and Bioengineering*, 118(7), 2744–2758. https://doi.org/10.1002/BIT.27793

Rodrigues, M. E., Costa, A. R., Henriques, M., Azeredo, J., & Oliveira, R. (2010). Technological progresses in monoclonal antibody production systems. *Biotechnology Progress*, 26(2), 332–351. https://doi.org/10.1002/BTPR.348

Shang, W., Chen, C. Y., Lo, K., Payne, G. F., & Bentley, W. E. (2019). Chip modularity enables molecular information access from organ-on-chip devices with quality control. *Sensors and Actuators, B: Chemical*, 295, 30–39. https://doi.org/10.1016/j.snb.2019.05.030

Shukla, A. A., Wolfe, L. S., Mostafa, S. S., & Norman, C. (2017). Evolving trends in mAb production processes. *Bioengineering & Translational Medicine*, 2(1), 58–69. https://doi.org/10.1002/BTM2.10061

Steinmeyer, D. E., & McCormick, E. L. (2008). The art of antibody process development. *Drug Discovery Today*, 13(13–14), 613–618. https://doi.org/10.1016/J.DRUDIS.2008.04.005

VanArsdale, E., Pitzer, J., Payne, G. F., & Bentley, W. E. (2020). Redox electrochemistry to interrogate and control biomolecular communication, *iScience* (Vol. 23, p. 101545). Elsevier Inc.

VanArsdale, E., Pitzer, J., Wang, S., Stephens, K., Chen, C.-Y., Payne, G. F., & Bentley, W. E. (2022a). Enhanced electrochemical measurement of β-galactosidase activity in whole cells by coexpression of lactose permease, LacY. *Biotechniques*, 73(5), 251–255. https://doi.org/10.2144/btn-2022-0090

VanArsdale, E., Pitzer, J., Wang, S., Stephens, K., Chen, C. Y., Payne, G. F., & Bentley, W. E. (2022b). Electrogenetic signal transmission and propagation in coculture to guide production of a small molecule, tyrosine. *ACS Synthetic Biology*, 11(2), 877–887. https://doi.org/10.1021/ACSSYNBIO.1C00522/SUPPL_FILE/SB1C00522_SI_001.PDF

VanArsdale, E., Tsao, C., Liu, Y., Chen, C., Payne, G. F., & Bentley, W. E. (2019). Redox-Based synthetic biology enables electrochemical detection of the herbicides dicamba and roundup via rewired *escherichia coli*. *ACS Sensors*, 4(5), 1180–1184. https://doi.org/10.1021/acssensors.9b00085

Wang, S., Tsao, C. Y., Motabar, D., Li, J., Payne, G. F., & Bentley, W. E. (2021). A redox-based autoinduction strategy to facilitate expression of 5xCys-tagged proteins for electrobiofabrication. *Frontiers in Microbiology*, 12, 14731473. https://doi.org/10.3389/FMICB.2021.675729/BIBTEX

Wu, A. M., Wu, J. H., Singh, T., Lai, L. J., Yang, Z., & Herp, A. (2006). Recognition factors of *Ricinus communis* agglutinin 1 (RCA1). *Molecular Immunology*, 43(10), 1700–1715. https://doi.org/10.1016/J.MOLIMM.2005.09.008

SUPPORTING INFORMATION

Additional supporting information can be found online in the Supporting Information section at the end of this article.